

Magnetic reconnection mediated by hyper-resistive plasmoid instability

Yi-Min Huang,^{1,2,3,*} A. Bhattacharjee,^{1,2,3} and Terry G. Forbes⁴

¹*Center for Integrated Computation and Analysis of Reconnection and Turbulence*

²*Center for Magnetic Self-Organization in Laboratory and Astrophysical Plasmas*

³*Max Planck-Princeton Center for Plasma Physics and*

Princeton Plasma Physics Laboratory, Princeton, NJ 08543

⁴*Space Science Center, University of New Hampshire, Durham, NH 03824*

Abstract

Magnetic reconnection mediated by the hyper-resistive plasmoid instability is studied with both linear analysis and nonlinear simulations. The linear growth rate is found to scale as $S_H^{1/6}$ with respect to the hyper-resistive Lundquist number $S_H \equiv L^3 V_A / \eta_H$, where L is the system size, V_A is the Alfvén velocity, and η_H is the hyper-resistivity. In the nonlinear regime, reconnection rate becomes nearly independent of S_H , the number of plasmoids scales as $S_H^{1/2}$, and the secondary current sheet length and width both scale as $S_H^{-1/2}$. These scalings are consistent with a heuristic argument assuming secondary current sheets are close to marginal stability. The distribution of plasmoids as a function of the enclosed flux ψ is found to obey a ψ^{-1} power law over an extended range, followed by a rapid fall off for large plasmoids. These results are compared with those from resistive magnetohydrodynamic studies.

* yiminh@princeton.edu

I. INTRODUCTION

Magnetic reconnection is arguably one of the most important processes in plasma physics, which provides a mechanism to release the energy stored in magnetic field and convert it to thermal energy or bulk plasma kinetic energy. It is generally believed to be the underlying mechanism that powers explosive events such as solar flares, magnetospheric substorms, and sawtooth crashes in fusion plasmas.[1, 2] The key challenge of magnetic reconnection theory applied to these events is how energy can be released explosively in time scales that are very short compared with the characteristic resistive diffusion time scale.

Traditionally, it was widely accepted that magnetic reconnection in the resistive magnetohydrodynamics (MHD) model is described by the classical Sweet-Parker theory.[3, 4] Sweet-Parker theory predicts that reconnection rate scales as $S^{-1/2}$, where $S \equiv V_A L / \eta$ is the Lundquist number (here V_A is the upstream Alfvén speed, L is the reconnection layer length, and η is the resistivity). Because the Lundquist number S is usual very high (e.g. in solar corona $S \sim 10^{12} - 10^{14}$, assuming the classical Spitzer resistivity), the Sweet-Parker reconnection rate is too slow to account for energy release events. For this reason, research on fast reconnection in the past two decades has mostly focused on collisionless reconnection, which can yield reconnection rates as fast as $\sim 0.1V_A B$ (here B is the upstream magnetic field).[5] In order to trigger collisionless reconnection, the current sheet width has to first go down to kinetic scales such as the ion skin depth or ion thermal gyroradius.[6–11]

The super-Alfvénic plasmoid instability,[12] which is a secondary tearing instability acting on a Sweet-Parker current sheet, has drawn considerable interest in recent years. While the scaling features of this linear instability are surprising in their own right,[12–15] what is more important is that the instability leads to a nonlinear regime in which the reconnection rate becomes nearly independent of S ,[13, 16–18] in striking departure from the prediction of Sweet-Parker theory. Furthermore, the plasmoid instability causes fragmentation of the Sweet-Parker current sheet to smaller secondary current sheets, which allows collisionless reconnection to be triggered earlier than previously thought possible.[19–21]

Over the past few years, the linear analysis of the plasmoid instability mediated by resistivity has been extended by various authors to include Hall,[22] three dimensional (3D),[23] and shear flow effects.[24] Nonlinear evolution of the instability has also been extensively studied in two dimensional (2D) systems.[13, 16, 18, 25–31] The resistive plasmoid instability

in 2D is now relatively well understood. However, the resistive tearing mode is not the only mechanism that causes plasmoid formation. In fact, plasmoid formation has been found to be ubiquitous in large scale reconnection simulations, regardless of the underlying physical models. [19, 32–36]

In this work, we explore the consequences of hyper-resistivity on magnetic reconnection mediated by the plasmoid instability. In this model, the Ohm’s law assumes the form $\mathbf{E} = -\mathbf{u} \times \mathbf{B} - \eta_H \nabla^2 \mathbf{J}$, where η_H is the hyper-resistivity. The origin of hyper-resistivity has been attributed to anomalous electron viscosity due to micro-scale field line stochasticity as well as tearing-mode turbulence.[37–43] This paper is organized as follows. The linear theory of the instability is established in Sec. II, where the scaling of the linear growth rate is derived. Sec. III presents the results from nonlinear simulations. First we verify the scaling of the linear growth rate, then move on to study the effects on magnetic reconnection when the instability has evolved into fully nonlinear regime. We focus on scalings of reconnection rate, the number of plasmoids, and the sizes of secondary current sheets. We give a heuristic justification for the scalings. Finally, we examine the statistical distribution of the magnetic flux contained in plasmoids, which is a topic of considerable interest in recent years. The results from both linear and nonlinear studies are summarized and discussed in Sec. IV, and comparisons are made with the plasmoid instability in resistive MHD.

II. LINEAR THEORY

The linear analysis of the plasmoid instability in resistive MHD was first carried out by Loureiro *et al.*[12] The analysis shows that the maximum growth rate γ_{max} scales as $S^{1/4}V_A/L$, and the number of plasmoids scales as $S^{3/8}$. Subsequently, it was shown that these scalings emerge directly from the classic tearing mode dispersion relation,[44] by taking into account the property that the width of the Sweet-Parker current sheet δ_{CS} scales as $L/S^{1/2}$. [13, 45] Here we follow the latter approach for the hyper-resistive plasmoid instability. To do that we need two ingredients: a generalization of the Sweet-Parker theory and a linear tearing mode theory with hyper-resistivity in place of resistivity.

The generalization of Sweet-Parker theory[3, 4] with hyper-resistivity is straightforward. Let u_i and u_o be the inflow speed and the outflow speed, respectively. The conditions for

conservation of mass and energy remains unchanged, which give

$$u_i L \sim u_o \delta_{CS}, \quad (1)$$

$$\rho u_o^2 \sim B^2. \quad (2)$$

Here ρ is the plasma density, B is the magnetic field, and we have neglected numerical factors of $O(1)$. The only deviation from the resistive Sweet-Parker theory comes from the Ohm's law, which is now $\mathbf{E} = -\mathbf{u} \times \mathbf{B} - \eta_H \nabla^2 \mathbf{J}$. Under quasi-steady condition, the out-of-plane electric field is spatially uniform, which gives the following condition

$$u_i B \sim \eta_H \nabla^2 J \sim \eta_H \frac{B}{\delta_{CS}^3}, \quad (3)$$

where we have made use of the relations $J \sim B/\delta_{CS}$ and $\nabla^2 \sim 1/\delta_{CS}^2$. From Eqs. (1) – (3), the following scaling relations are obtained:

$$u_o \sim \frac{B}{\sqrt{\rho}} \sim V_A, \quad (4)$$

$$\delta_{CS} \sim \frac{L}{S_H^{1/4}}, \quad (5)$$

and

$$u_i \sim S_H^{-1/4} V_A, \quad (6)$$

where S_H is the hyper-resistive Lundquist number defined as

$$S_H \equiv \frac{L^3 V_A}{\eta_H}. \quad (7)$$

The linear dispersion relation of hyper-resistive tearing mode has been derived by Aydemir.[46] Here we outline the analysis to keep this paper self-contained. For simplicity, the plasma is assumed to be incompressible with a uniform density. In two-dimensional (2D) Cartesian coordinates (x, z) , the plasma flow \mathbf{u} and the magnetic field \mathbf{B} can be expressed in terms of the stream function ϕ and the flux function ψ as $\mathbf{u} = \nabla\phi \times \hat{\mathbf{y}}$ and $\mathbf{B} = \nabla\psi \times \hat{\mathbf{y}}$, and the system can be described by the well-known reduced MHD equations.[43, 47, 48] Consider an equilibrium magnetic field $\mathbf{B} = B_x(z)\hat{\mathbf{x}}$, with $V_A(z)$ being the corresponding Alfvén speed profile. Assuming linear perturbations of the form $\tilde{\phi} = \tilde{\phi}(z)e^{ikx+\gamma t}$ and $\tilde{\psi} = \tilde{\psi}(z)e^{ikx+\gamma t}$, where γ is the growth rate and k is the wavenumber along the x direction, the linearized reduced MHD equations with hyper-resistivity are:

$$\gamma \mathcal{D} \tilde{\phi} = ik V_A \mathcal{D} \tilde{\psi} - ik V_A'' \tilde{\psi}, \quad (8)$$

$$\gamma\tilde{\psi} = ikV_A\tilde{\phi} - \eta_H\mathcal{D}^2\tilde{\psi}. \quad (9)$$

Here primes denote d/dz and the operator $\mathcal{D} \equiv d^2/dz^2 - k^2$. We further assume that $z = 0$ is the resonant surface, where $V_A = 0$.

Away from $z = 0$, the effect of hyper-resistivity is negligible. Therefore, in the outer region $\tilde{\phi} \simeq \gamma\tilde{\psi}/ikV_A$, which can be used in Eq. (8) to eliminate $\tilde{\phi}$. It follows that if we assume $\gamma^2 \ll k^2V_A^2$, the plasma inertia (left hand side of Eq. (8)) is negligible. Hence, in the outer region, the perturbed flux function $\tilde{\psi}_o$ is governed by

$$\left(\mathcal{D} - \frac{V_A''}{V_A}\right)\tilde{\psi}_o \simeq 0. \quad (10)$$

The solution of Eq. (10) is subject to appropriate outer boundary condition, e.g. $\tilde{\psi}_o \rightarrow 0$ at infinity if the global length scale of the domain along the z direction under consideration is much larger than the current sheet width. In general, the solutions of $\tilde{\psi}_o$ from both regions $z > 0$ and $z < 0$ will not match smoothly at $z = 0$. The mismatch in the slope of $\tilde{\psi}_o$ is characterized by the tearing stability index [49]

$$\Delta' \equiv \left. \frac{\tilde{\psi}'_o}{\tilde{\psi}_o} \right|_{0^-}^{0^+}, \quad (11)$$

which is completely determined by the equilibrium profile and the wave number k .

Because the outer solutions do not match smoothly at $z = 0$, a boundary layer exists around $z = 0$. In the inner region around $z = 0$, a separate set of boundary layer equations

$$\gamma\tilde{\phi}'' = ikV_A'(0)x\tilde{\psi}'', \quad (12)$$

$$\gamma\tilde{\psi} = ikV_A'(0)x\tilde{\phi} - \eta_H\tilde{\psi}'''' \quad (13)$$

are solved. Asymptotic matching of the inner and outer solutions give the linear growth rate. Interested readers are referred to Ref. [46] for a detailed asymptotic analysis. It is instructive, however, to employ a simple heuristic argument that gives correct scalings of the linear growth rate, as follows.

Let a be the width of the equilibrium current sheet and δ be the width of the boundary layer. Tearing modes are often classified into the so-called constant- ψ and nonconstant- ψ regimes, depending on whether $\tilde{\psi}$ is approximately constant or not within the boundary layer. In the constant- ψ regime, the variation of $\tilde{\psi}'$ is approximately $\tilde{\psi}\Delta'$ across the boundary

layer. Hence, we may estimate $\tilde{\psi}'' \sim \tilde{\psi} \Delta' / \delta$ and $\tilde{\psi}'''' \sim \tilde{\psi} \Delta' / \delta^3$. Also $\tilde{\phi}''$ may be estimated as $\tilde{\phi} / \delta^2$, and $V_A'(0) \sim V_A / a$. Balancing terms in Eqs. (12) and (13) yields

$$\gamma \tilde{\phi} / \delta^2 \sim k \frac{V_A}{a} \delta \frac{\Delta' \tilde{\psi}}{\delta}, \quad (14)$$

$$\gamma \tilde{\psi} \sim k \frac{V_A}{a} \delta \tilde{\phi} \sim \eta_H \frac{\Delta' \tilde{\psi}}{\delta^3}. \quad (15)$$

Solving Eqs. (14) and (15) yields the scalings of δ and γ . The results are

$$\delta \sim S_{Ha}^{-2/9} (\Delta' a)^{1/9} (ka)^{-2/9} a \quad (16)$$

and

$$\gamma \sim S_{Ha}^{-1/3} (\Delta' a)^{2/3} (ka)^{2/3} (V_A / a), \quad (17)$$

where

$$S_{Ha} \equiv \frac{\alpha^3 V_A}{\eta_H} \quad (18)$$

is the hyper-resistive Lundquist based on the length scale of the equilibrium current sheet width a . For the commonly employed Harris sheet profile with $V_A \propto \tanh(z/a)$, the tearing stability index is given by

$$\Delta' = \frac{2}{ka^2} (1 - (ka)^2). \quad (19)$$

Using Eq. (19) in Eqs. (23) and (24) yields

$$\delta \sim S_{Ha}^{-2/9} (ka)^{-1/3} (1 - (ka)^2)^{1/9} a \quad (20)$$

and

$$\gamma \sim S_{Ha}^{-1/3} (1 - (ka)^2)^{2/3} (V_A / a) \quad (21)$$

in the constant- ψ regime. More precisely, the $O(1)$ numerical factor in Eq. (21) can be determined by an asymptotic matching calculation,[46] which gives

$$\gamma \simeq (2/\pi)^{2/3} S_{Ha}^{-1/3} (1 - (ka)^2)^{2/3} (V_A / a). \quad (22)$$

In the nonconstant- ψ regime, $\tilde{\psi}$ varies significantly within the boundary layer, and we may estimate $\tilde{\psi}'' \sim \tilde{\psi} / \delta^2$ and $\tilde{\psi}'''' \sim \tilde{\psi} / \delta^4$. Following the same procedure of balancing terms in Eqs. (12) and (13) yields

$$\delta \sim S_{Ha}^{-1/5} (ka)^{-1/5} a \quad (23)$$

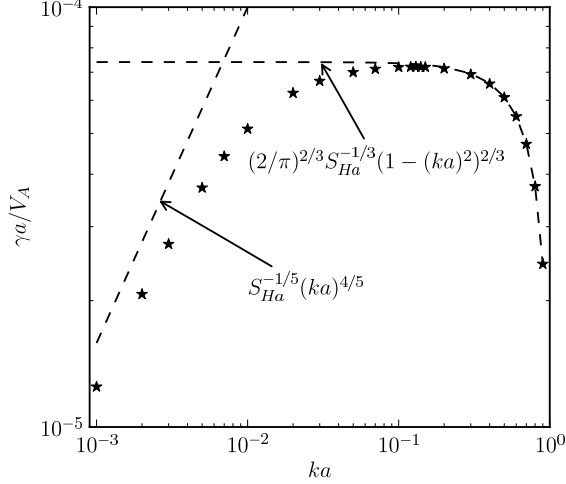


Figure 1. The dimensionless growth rate $\gamma a/V_A$ as a function of ka , for a Harris sheet profile with $S_{Ha} = 10^{12}$. Markers denote values obtained by numerically solving the eigenvalue problem. Dashed lines are theoretical predictions for the constant- ψ and nonconstant- ψ branches, Eqs. (22) and (24).

and

$$\gamma \sim S_{Ha}^{-1/5} (ka)^{4/5} (V_A/a). \quad (24)$$

The transition wavenumber from the constant- ψ regime to the nonconstant- ψ regime may be estimated from the self-consistency of the constant- ψ assumption, as follows. The variation of $\tilde{\psi}$ within the boundary layer may be estimated as $\Delta\tilde{\psi} \sim \tilde{\psi}'\delta \sim \tilde{\psi}\Delta'\delta$. Therefore, $\tilde{\psi}$ being approximately constant requires $\Delta\tilde{\psi} \ll \tilde{\psi}$, i.e. $\Delta'\delta \ll 1$. From Eqs. (19) and (23), the self-consistency criterion $\Delta'\delta \ll 1$ requires $ka \gg S_{Ha}^{-1/6}$, assuming $S_{Ha}^{-1/6} \ll 1$. Therefore, we expect that the transition occurs when $ka \sim S_{Ha}^{-1/6}$. Note that γ is a monotonically decreasing function of ka in the constant- ψ regime, and a monotonically increasing function of ka in the nonconstant- ψ regime. At the transition wavenumber the growth rates from two branches coincide, which gives the peak growth rate $\gamma_{max} \sim S_{Ha}^{-1/3} (V_A/a)$.

These scalings are verified by numerically solving the eigenvalue problem, Eqs. (8) and (9). Figure 1 shows the dimensionless growth rate $\gamma a/V_A$ as a function of ka , for a Harris sheet profile with $S_{Ha} = 10^{12}$. The numerical values agree with the analytic predictions remarkably well. Likewise, Figure 2 shows the scaling of the maximum dimensionless growth rate $\gamma_{max} a/V_A$ with S_{Ha} . The numerical values agree well with the theoretical scaling relation $\gamma_{max} a/V_A \sim S_{Ha}^{-1/3}$.

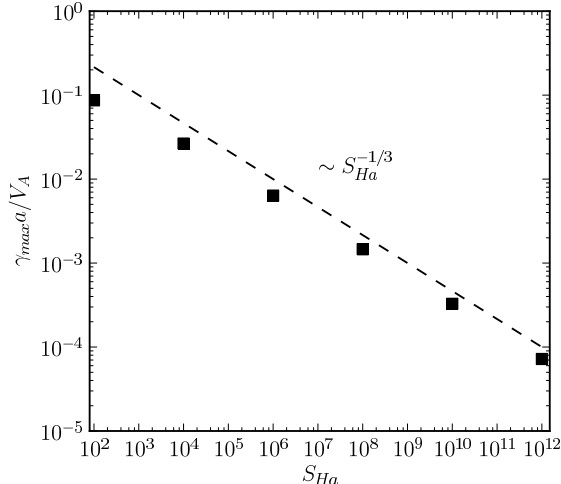


Figure 2. Scaling of the maximum dimensionless growth rate $\gamma_{max}a/V_A$ with S_{Ha} , for a Harris sheet profile. Markers denote values obtained by numerically solving the eigenvalue problem. Dashed line is the theoretical prediction $\gamma_{max}a/V_A \sim S_{Ha}^{-1/3}$.

Now we have all the ingredients for the linear theory of hyper-resistive plasmoid instability. Substituting the hyper-resistive Sweet-Parker current sheet width $\delta_{CS} \sim L/S_H^{1/4}$ for the current sheet width a in the linear tearing mode theory, we obtain the following relation between S_H and S_{Ha}

$$S_{Ha} \sim S_H^{1/4}. \quad (25)$$

Also the maximum growth rate scales as

$$\gamma_{max} \sim S_H^{1/6} (V_A/L). \quad (26)$$

As such, the instability growth rate increases for higher S_H , similar to the resistive counterpart. The transition from constant- ψ regime to nonconstant- ψ regime occurs at $kL \sim S_H^{5/24}$. Unlike the case of the resistive plasmoid instability, we are not able to obtain a precise scaling for the number of plasmoids in the hyper-resistive case, for the following reason. In the resistive plasmoid instability, the scaling of the number of plasmoids can be inferred from the wavenumber of the fastest growing mode, which coincides with the transition wavenumber from the constant- ψ regime to the nonconstant- ψ regime.[12, 13, 45] That is not the case with hyper-resistivity. For hyper-resistive tearing modes, the growth rate is approximately constant within the range $S_{Ha}^{-1/6} \ll ka \ll 1$ (see, for example, Figure 1), or equivalently within the range $S_H^{5/24} \ll kL \ll S_H^{1/4}$, and the notion of fastest growing wavenumber loses

its significance.

There are some subtleties in making qualitative comparisons between the resistive and hyper-resistive plasmoid instabilities because the mechanisms that break the frozen-in condition are quite different in the two cases. A meaningful comparison may be made by rewriting the scaling laws in terms of the aspect ratio L/δ_{CS} of the primary Sweet-Parker current sheet, which is a common feature for both models. For the resistive case, the maximum growth rate scales as

$$\gamma_{max} \sim \left(\frac{L}{\delta_{CS}} \right)^{1/2} \frac{V_A}{L}, \quad (27)$$

and the fastest growing mode has a dimensionless wavenumber

$$kL \sim \left(\frac{L}{\delta_{CS}} \right)^{3/4}. \quad (28)$$

On the other hand, for the hyper-resistive plasmoid instability, the maximum growth rate scales as

$$\gamma_{max} \sim \left(\frac{L}{\delta_{CS}} \right)^{2/3} \frac{V_A}{L}, \quad (29)$$

and the growth rate peaks when kL is within the range

$$\left(\frac{L}{\delta_{CS}} \right)^{5/6} \ll kL \ll \frac{L}{\delta_{CS}}. \quad (30)$$

From these scaling laws we may conclude that the hyper-resistive plasmoid instability has a higher growth rate and prefers shorter wavelengths as compared to the resistive one. Therefore, the hyper-resistive plasmoid instability is even more explosive, and more efficient in generating copious plasmoids, than the resistive plasmoid instability.

III. NUMERICAL SIMULATIONS

The resistive plasmoid instability is of great interest because it leads to a nonlinear regime where magnetic reconnection is drastically different from the Sweet-Parker model. A pivotal question is how the hyper-resistive plasmoid instability affects reconnection in the nonlinear regime. To address this question, we employ the same simulation setup of two coalescing magnetic islands as in Ref. [16]. The governing equations are identical to the ones before, except that resistivity is now replaced by hyper-resistivity. An isothermal equation of state is assumed for simplicity. In normalized units, the simulation box is a

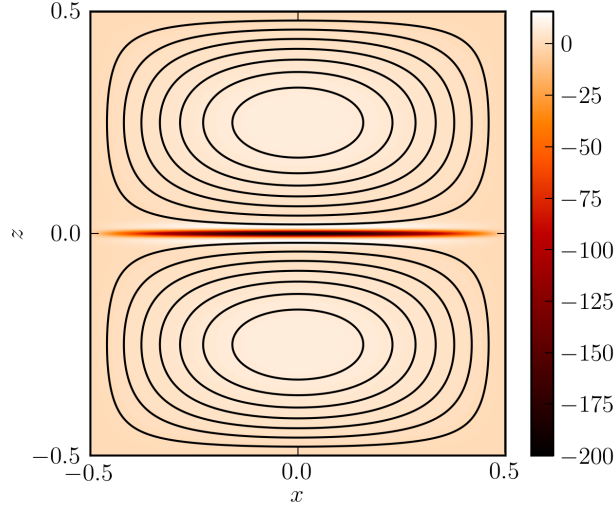


Figure 3. (Color online) The initial current density distribution, overlaid with magnetic field lines.

square in the domain $(x, z) \in [-1/2, 1/2] \times [-1/2, 1/2]$. The initial magnetic field is given by $\mathbf{B}_0 = \nabla\psi_0 \times \hat{\mathbf{y}}$, where $\psi_0 = \tanh(z/h) \cos(\pi x) \sin(2\pi z)/2\pi$. The parameter h , which is set to 0.01 for all simulations, determines the initial current layer width. The initial plasma density ρ is approximately 1, and the plasma temperature T is 3. The density profile has a weak nonuniformity such that the initial condition is approximately force-balanced. The initial peak magnetic field and Alfvén speed are both approximately unity. Therefore, the hyper-resistive Lundquist number $S_H = L^3 V_A / \eta_H$ is simply $1/\eta_H$. The plasma beta $\beta \equiv p/B^2 = 2\rho T/B^2$ is greater than 6 everywhere. Perfectly conducting and free slipping boundary conditions are imposed along both x and z directions. Specifically, we have $\psi = 0$, $\mathbf{u} \cdot \hat{\mathbf{n}} = 0$, and $\hat{\mathbf{n}} \cdot \nabla(\hat{\mathbf{n}} \times \mathbf{u}) = 0$ (here $\hat{\mathbf{n}}$ is the unit normal vector to the boundary). Only the upper half of the domain ($z \geq 0$) is simulated, and the solutions in the lower half are inferred by symmetries. We employ a uniform mesh along the x direction, whereas the grid points along the z direction are strongly concentrated around $z = 0$ to better resolve the reconnection layer. The highest resolution is 16000 grid points along the x direction and 1000 grid points along the z direction, with the smallest grid size $\Delta z = 1.8 \times 10^{-5}$. Figure 3 shows the initial current density distribution, overlaid with magnetic field lines. As the simulation proceeds, the current layer first thins down and forms the primary hyper-resistive Sweet-Parker layer. Subsequently, the primary current layer may become unstable to the plasmoid instability if S_H is above a threshold $S_{Hc} \simeq 10^{10}$. We show snapshots of a simulation with $S_H = 10^{14}$ in Fig. 4.

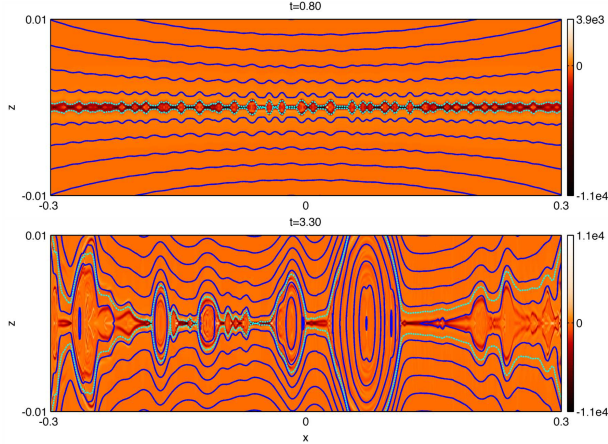


Figure 4. (Color online) Snapshots of the out-of-plane current profile, overlaid with magnetic field lines, from a $S_H = 10^{14}$ run. Dashed lines represent separatrices separating the two primary merging islands that drive the reconnection. The top panel shows the instability in the early stage, and the bottom panel shows the fully developed nonlinear stage.

A. Verification of Linear Theory

Before we study magnetic reconnection in fully nonlinear regime for this system, we first verify the prediction $\gamma_{max} \sim S_H^{1/6} (V_A/L)$ from the linear analysis. One difficulty in measuring the linear growth rate is due to the fact that we do not start the simulation with a Sweet-Parker current sheet. Rather, the Sweet-Parker current sheet is established self-consistently during the current sheet thinning phase. Therefore, the standard technique of adding a small perturbation to an initial equilibrium and measuring the growth rate as the perturbation grows does not apply here. The problem is that most physical quantities evolve quite substantially during the current sheet thinning phase before onset of the plasmoid instability, and it is difficult to filter out the variations that are not due to the growth of the plasmoid instability. This difficulty is overcome by looking at the component B_z along the central part of the reconnection layer $z = 0$, where B_z is identically zero initially and remains small before onset of the plasmoid instability. After the onset, the component B_z develops fluctuations which rapidly grow as time proceeds. To obtain the linear growth rate, we integrate B_z^2 at the central part of the current sheet along $z = 0$, from $x = -1/4$ to $1/4$ at each time. The magnitude of $f(t) \equiv \int_{-1/4}^{1/4} B_z^2(t) dx$ remains small before onset of the plasmoid instability, and increases abruptly after the onset. The linear growth rate γ

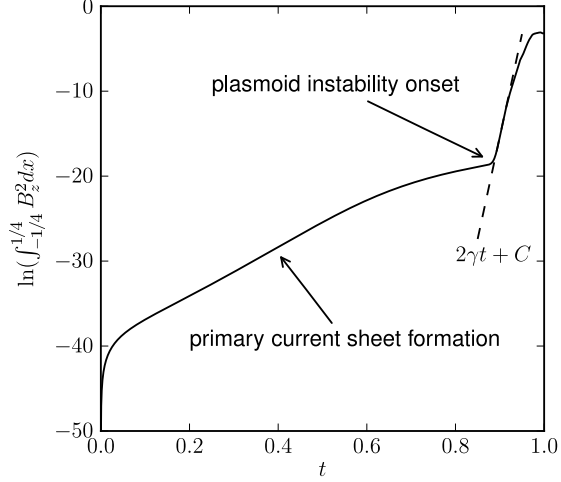


Figure 5. Measurement of the linear growth rate for the case $S_H = 10^{14}$.

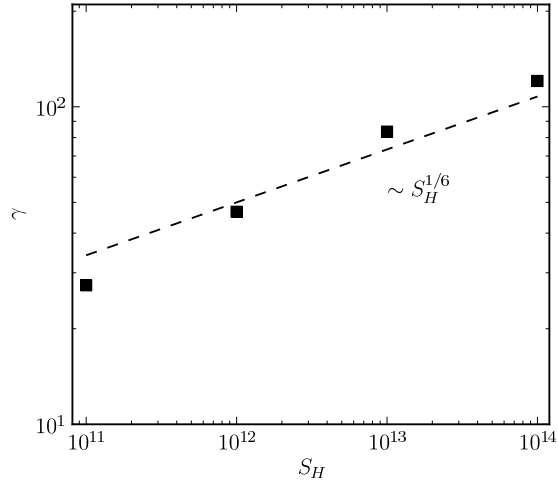


Figure 6. Scaling of the linear growth rate with respect to S_H . The dashed line is the prediction from the linear theory.

can be obtained by fitting $\ln(f(t))$ to a linear function $\ln(f(t)) \simeq 2\gamma t + c$ during the period the plasmoid instability exhibits approximately linear growth. This procedure is illustrated in Figure 5 for the case $S_H = 10^{14}$. We measure the linear growth rates for cases with S_H ranging from 10^{11} to 10^{14} . Figure 6 shows the scaling of γ with respect to S_H . The results are in good agreement with the prediction $\gamma_{max} \sim S_H^{1/6} (V_A/L)$.

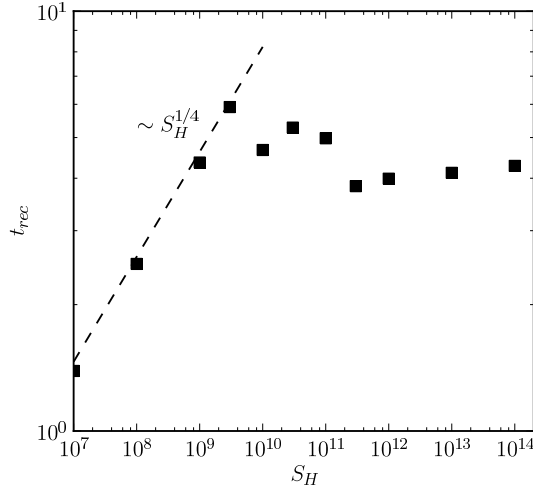


Figure 7. Scaling of the time to reconnect 25% of the initial magnetic flux with respect to S_H .

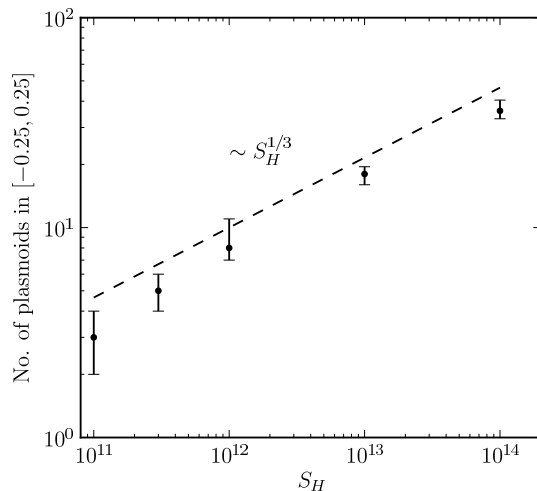


Figure 8. Scaling of the number of the plasmoids within $x \in [-0.25, 0.25]$ with respect to S_H .

B. Scaling Laws in Nonlinear Regime

The next step is to establish scaling laws in the nonlinear regime of hyper-resistive plasmoid instability, as we have done in a previous study [16] for the resistive counterpart. For nonlinear simulations, a low amplitude random forcing is included to mimic thermal noise in real systems. In Ref. [16], it is found that the result depends only weakly on the amplitude of random forcing. For this reason, we set the random forcing amplitude at a fixed level $\epsilon = 10^{-4}$. The readers are referred to Ref. [16] for details of how the amplitude ϵ is related to the energy input due to the random forcing and how the random forcing is implemented

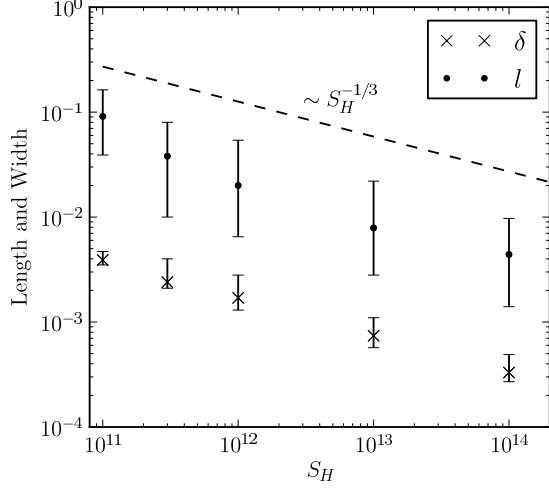


Figure 9. Scalings of the length l and width δ of secondary current sheets with respect to S_H .

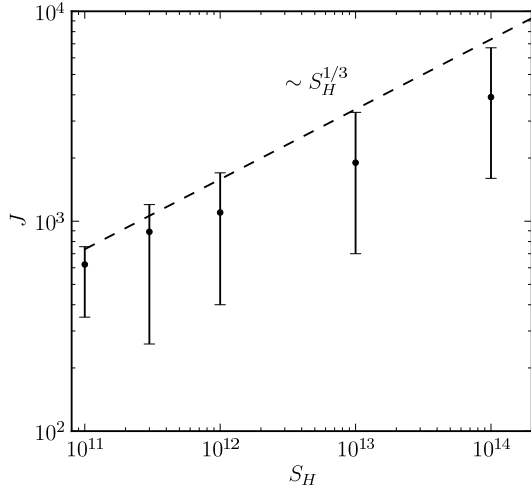


Figure 10. Scaling of the out-of-plane current density J with respect to S_H .

numerically.

We employ the same diagnostics as in Ref. [16]. To quantify the speed of reconnection, we measure the time it takes to reconnect 25% of the magnetic flux within the two merging islands, which is denoted as t_{rec} . Figure 7 shows the scaling of t_{rec} with respect to S_H . For lower S_H , the reconnection time scales as $t_{rec} \sim S_H^{1/4}$, as expected from the hyper-resistive Sweet-Parker theory. When S_H is above a critical value $S_{Hc} \simeq 10^{10}$, the plasmoid instability sets in and the reconnection time t_{rec} becomes nearly independent of S_H . In normalized units, the global characteristic values for V_A and B are approximately 1, and 25% of the initial magnetic flux inside each of the islands is 0.04, therefore the normalized average

reconnection rate is given by

$$\frac{1}{BV_A} \left\langle \frac{d\psi}{dt} \right\rangle = \frac{0.04}{t_{rec}}. \quad (31)$$

In the regime $S_H > 10^{10}$, $t_{rec} \simeq 4$ to 5 from our simulations and the normalized reconnection rate is in the range 0.008 to 0.01. As such, the normalized reconnection rates here are on par with those in resistive MHD models. [13, 16, 50]

In Ref. [16], scaling laws for the number of plasmoids, current sheet lengths and widths, and current density have been deduced from simulation data. It was shown that those scaling laws may be understood by a heuristic argument that considers the reconnection layer as a chain of plasmoids connected by marginally stable current sheets. The same argument may be carried over to the hyper-resistive plasmoid instability, as follows. For given η_H and V_A , the critical length of a marginally stable current layer is $L_c \sim (S_{Hc}\eta_H/V_A)^{1/3} \sim L(S_{Hc}/S_H)^{1/3}$. Therefore we expect the number of plasmoids in the nonlinear regime n_p to scale like $n_p \sim L/L_c \sim (S_H/S_{Hc})^{1/3}$. Furthermore, the width of the marginally stable current sheet $\delta_c \sim L_c/S_{Hc}^{1/4} \sim LS_{Hc}^{1/12}/S_H^{1/3}$, and the current density $J \sim B/\delta_c \sim (B/L)S_{Hc}^{-1/12}S_H^{1/3}$. Finally, we may estimate the reconnection rate by $\eta_H J/\delta_c^2 \sim \eta_H B/\delta_c^3 \sim BV_A/S_{Hc}^{1/4}$, which is independent of S_H . This prediction of reconnection rate being independent of S_H is consistent with our results, shown in Figure 7. Likewise, the predictions that the number of plasmoids scales as $S_H^{1/3}$, the current sheet width and length both scale as $S_H^{-1/3}$, and the current density scales as $S_H^{1/3}$ are also borne out by our simulation data, shown in Figures 8, 9, and 10. These data are collected from time slices during the period to reconnect 25% of the initial flux, and only plasmoids and secondary current sheets within the domain $x \in [-0.25, 0.25]$ are considered. Because the number of plasmoids at a given snapshot varies in time, in Figure 8 the medians are plotted, and the error bars denote the first and third quartiles. Likewise, current sheets also vary in length, width, and current density from one to another. The data points and error bars in Fig. 9, and Fig. 10 also denote the medians and the quartiles.

C. Statistical Distribution of Plasmoids

Seeking statistical descriptions of plasmoids has been a topic of considerable interest in recent years, [17, 18, 45, 51–53] partly due to the possible link between plasmoids and energetic particles.[54–56] In our recent work with resistive MHD, it was found numerically that

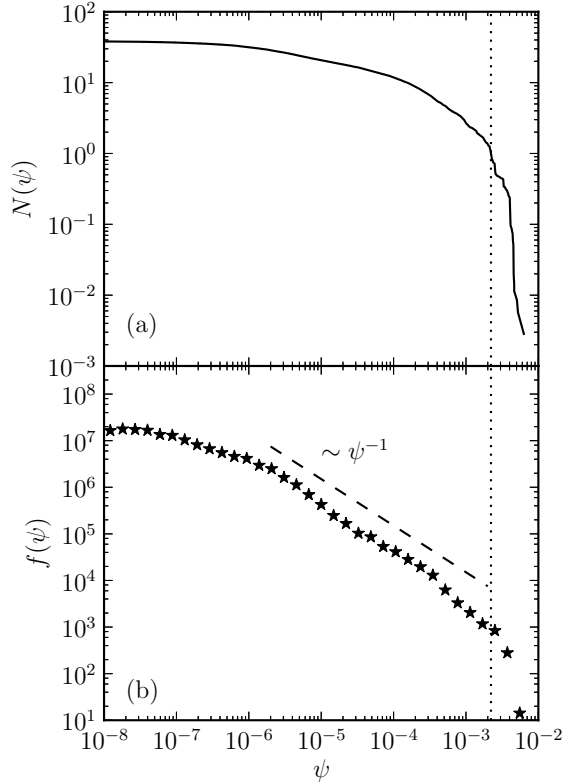


Figure 11. (a) Cumulative distribution function $N(\psi)$ and (b) probability distribution function $f(\psi)$ from a $S_H = 10^{14}$ simulation. The vertical dotted line denotes where $N(\psi) = 1$, indicating where the dominant loss mechanism switches from coalescence to advection.

the distribution function $f(\psi)$ of magnetic flux ψ inside plasmoids exhibits a $f(\psi) \sim \psi^{-1}$ power-law distribution over an extended range, followed by an exponential tail for large plasmoids. A theoretical model was proposed that yields results consistent with the numerical simulations.[45, 53] It has been clarified that the transition from the power-law distribution to the exponential tail is due to the dominant plasmoid loss mechanism switching from coalescence to advection. This transition typically occurs when the cumulative distribution function $N(\psi) \equiv \int_{\psi}^{\infty} f(\psi') d\psi'$ obeys the approximately inequality $N \lesssim 1$, i.e. for the very largest plasmoids in each snapshot. Because the theoretical model only relies on the key assumption that secondary current sheets between plasmoids are close to marginal stability and a few general assumptions regarding coalescence and advection of plasmoids, the model can be readily adapted to the case of hyper-resistive plasmoid instability. Therefore, we expect plasmoids in hyper-resistive MHD model to follow a similar distribution. That indeed appears to be the case. Figure 11 shows the cumulative distribution function $N(\psi)$ and

	Resistive	Hyper-Resistive
γ_{max}	$\sim \Lambda^{1/2}$	$\sim \Lambda^{2/3}$
κ_{max}	$\sim \Lambda^{3/4}$	$\Lambda^{5/6} \ll \kappa_{max} \ll \Lambda$
n_p	$\sim \Lambda^2$	$\sim \Lambda^{4/3}$
δ and l	$\sim \Lambda^{-2}$	$\sim \Lambda^{-4/3}$
J	$\sim \Lambda^2$	$\sim \Lambda^{4/3}$
Reconnection Rate	$\simeq 10^{-2}V_AB$	$\simeq 10^{-2}V_AB$
Plasmoid Distribution	$f(\psi) \sim \psi^{-1}$	$f(\psi) \sim \psi^{-1}$

Table I. Comparison between resistive and hyper-resistive plasmoid instabilities. The scaling laws are expressed in terms of the aspect ratio $\Lambda = L/\delta_{CS}$. Here γ_{max} is the peak linear growth rate; $\kappa_{max} \equiv k_{max}L$ is the fastest growing wave number; n_p is the number of plasmoids in nonlinear regime; δ and l are the thickness and length of secondary current sheets; and J is the current density.

the distribution function $f(\psi)$ from a $S_H = 10^{14}$ simulation. The data set comprises 13486 plasmoids collected from 352 snapshots during the period of reconnecting 25% of the initial magnetic flux. The distribution function $f(\psi)$ clearly exhibits an extended $f(\psi) \sim \psi^{-1}$ power-law regime in the range between $\psi \sim 10^{-6}$ and $\psi \sim 10^{-3}$. Above $\psi \sim 10^{-3}$ the distribution makes a transition to a more rapid falloff. And this transition approximately coincides the vertical dotted line, which denotes where $N(\psi) = 1$, indicating a switch of the dominant loss mechanism from coalescence to advection. These features are qualitatively similar to the ones with resistive plasmoid instability.

IV. SUMMARY AND DISCUSSION

In summary, we have carried out a linear instability analysis and nonlinear simulations of the plasmoid instability when hyper-resistivity is the mechanism of breaking field lines. We have found that the hyper-resistive plasmoid instability is qualitatively similar to the resistive plasmoid instability, although they follow different scaling laws both linearly and nonlinearly. In the plasmoid-unstable regime, the reconnection rate is found to be nearly independent of the hyper-resistive Lundquist number S_H instead of following the predicted

$\sim S_H^{-1/4}$ scaling obtained by assuming a stable, extended current layer. The reconnection rate in high- S_H regime is approximately $0.01V_A B$, which is similar to the value obtained with the resistive plasmoid instability. The scaling laws in the nonlinear regime can be heuristically derived by assuming secondary current sheets between plasmoids are close to marginally stable, even though that assumption is clearly oversimplified. The distribution of plasmoid magnetic flux is found to obey a $f(\psi) \sim \psi^{-1}$ power law over an extended range, followed by a rapid falloff for large plasmoids — similar to the result obtained for the resistive plasmoid instability.

Table I summarizes the comparison between resistive and hyper-resistive plasmoid instabilities. Here the scaling laws are expressed in terms of the aspect ratio $\Lambda = L/\delta_{CS}$, which is a common feature of both models. The aspect ratio scales with respect to the resistive and hyper-resistive Lundquist numbers as $\Lambda \sim S^{1/2}$ and $\Lambda \sim S_H^{1/4}$, respectively. From these scaling relations, we can see that for the same aspect ratio Λ , the hyper-resistive plasmoid instability has a higher peak linear growth rate, and shorter wavelengths. Therefore, the hyper-resistive plasmoid instability will set in more rapidly, with more plasmoids at the early stage, compared to the resistive case. However, after the plasmoid instability has developed into fully nonlinear regime, more plasmoids will be present in the resistive case. The reason is that resistivity is less effective in smoothing out small-scale structure, which allows current sheet fragmentation to cascade down to deeper level.

The results in this paper may be relevant to the solar atmosphere, where hyper-resistivity has been proposed as a possible mechanism for corona heating.[57] In addition, some recent studies have found that current sheets formed after coronal mass ejection (CME) events have thicknesses far broader than classical or anomalous resistivity would predict, and it was suggested that hyper-resistivity may be the cause.[58, 59] Recently, a comparison of plasmoid distributions in post-CME current sheets obtained from both solar observation and resistive MHD simulation has been made.[60] However, because plasmoid distributions obtained from both resistive MHD and hyper-resistive MHD models are essentially identical, statistical study of plasmoid distribution alone will not be able to distinguish the two models. This conclusion calls for other measures that can better tell apart different models. The various scaling relations obtained in this paper may be able to provide other insights on how this can be done.

ACKNOWLEDGMENTS

This work is supported by the Department of Energy, Grant No. DE-FG02-07ER46372, under the auspice of the Center for Integrated Computation and Analysis of Reconnection and Turbulence (CICART), the National Science Foundation, Grant No. PHY-0215581 (PFC: Center for Magnetic Self-Organization in Laboratory and Astrophysical Plasmas), NASA Grant Nos. NNX09AJ86G and NNX10AC04G, and NSF Grant Nos. ATM-0802727, ATM-090315 and AGS-0962698. YMH is partially supported by a NASA subcontract to the Smithsonian Astrophysical Observatory's Center of Astrophysics, Grant No. NNM07AA02C. Computations were performed on facilities at National Energy Research Scientific Computing Center.

-
- [1] E. G. Zweibel and M. Yamada, *Annu. Rev. Astron. Astrophys.* **47**, 291 (2009).
 - [2] M. Yamada, R. Kulsrud, and H. Ji, *Rev. Mod. Phys.* **82**, 603 (2010).
 - [3] P. A. Sweet, *Nuovo Cimento Suppl.* **8**, 188 (1958).
 - [4] E. N. Parker, *J. Geophys. Res.* **62**, 509 (1957).
 - [5] J. Birn, J. F. Drake, M. A. Shay, B. N. Rogers, R. E. Denton, M. Hesse, M. Kuznetsova, Z. W. Ma, A. Bhattacharjee, A. Otto, and P. L. Pritchett, *J. Geophys. Res.* **106**, 3715 (2001).
 - [6] A. Y. Aydemir, *Phys Fluids B-Plasma Phys.* **4**, 3469 (1992).
 - [7] Z. W. Ma and A. Bhattacharjee, *Geophys. Res. Lett.* **23**, 1673 (1996).
 - [8] J. C. Dorelli and J. Birn, *J. Geophys. Res.* **108**, 1133 (2003).
 - [9] A. Bhattacharjee, *Annu. Rev. Astron. Astrophys.* **42**, 365 (2004).
 - [10] P. A. Cassak, M. A. Shay, and J. F. Drake, *Phys. Rev. Lett.* **95**, 235002 (2005).
 - [11] P. A. Cassak, J. F. Drake, and M. A. Shay, *Phys. Plasmas* **14**, 054502 (2007).
 - [12] N. F. Loureiro, A. A. Schekochihin, and S. C. Cowley, *Phys. Plasmas* **14**, 100703 (2007).
 - [13] A. Bhattacharjee, Y.-M. Huang, H. Yang, and B. Rogers, *Phys. Plasmas* **16**, 112102 (2009).
 - [14] R. Samtaney, N. F. Loureiro, D. A. Uzdensky, A. A. Schekochihin, and S. C. Cowley, *PRL* **103**, 105004 (2009).
 - [15] L. Ni, K. Germaschewski, Y.-M. Huang, B. P. Sullivan, H. Yang, and A. Bhattacharjee, *Phys. Plasmas* **17**, 052109 (2010).

- [16] Y.-M. Huang and A. Bhattacharjee, *Phys. Plasmas* **17**, 062104 (2010).
- [17] D. A. Uzdensky, N. F. Loureiro, and A. A. Schekochihin, *PRL* **105**, 235002 (2010).
- [18] N. F. Loureiro, R. Samtaney, A. A. Schekochihin, and D. A. Uzdensky, *Phys. Plasmas* **19**, 042303 (2012).
- [19] W. Daughton, V. Roytershteyn, B. J. Albright, H. Karimabadi, L. Yin, and K. J. Bowers, *Phys. Rev. Lett.* **103**, 065004 (2009).
- [20] L. S. Shepherd and P. A. Cassak, *Phys. Rev. Lett.* **105**, 015004 (2010).
- [21] Y.-M. Huang, A. Bhattacharjee, and B. P. Sullivan, *Phys. Plasmas* **18**, 072109 (2011).
- [22] S. D. Baalrud, A. Bhattacharjee, Y.-M. Huang, and K. Germaschewski, *Phys. Plasmas* **18**, 092108 (2011).
- [23] S. D. Baalrud, A. Bhattacharjee, and Y.-M. Huang, *Phys. Plasmas* **19**, 022101 (2012).
- [24] N. F. Loureiro, A. A. Schekochihin, and D. A. Uzdensky, *Phys. Rev. E* **87**, 013102 (2013).
- [25] P. A. Cassak and M. A. Shay, *Phys. Plasmas* **16**, 055704 (2009).
- [26] M. Bárta, J. Büchner, M. Karlický, and J. Skála, *Astrophys. J.* **737**, 24 (2011).
- [27] C. Shen, J. Lin, and N. A. Murphy, *Astrophys. J.* **737**, 14 (2011).
- [28] L. Ni, U. Ziegler, Y.-M. Huang, J. Lin, and Z. Mei, *Phys. Plasmas* **19**, 072902 (2012).
- [29] L. Ni, I. I. Roussev, J. Lin, and U. Ziegeler, *Astrophys. J.* **758**, 20 (2012).
- [30] Z. Mei, C. Shen, N. Wu, J. Lin, N. A. Murphy, and I. I. Roussev, *Mon. Not. R. Astr. Soc.* **425**, 2824 (2012).
- [31] H. Baty, *Phys. Plasmas* **19**, 092110 (2012).
- [32] J. F. Drake, M. Swisdak, K. M. Schoeffler, B. N. Rogers, and S. Kobayashi, *Geophysical Research Letters* **33**, L13105 (2006).
- [33] W. Daughton, J. Scudder, and H. Karimabadi, *Phys. Plasmas* **13**, 072101 (2006).
- [34] W. Daughton, V. Roytershteyn, H. Karimabadi, S. P. Gary, L. Yin, B. J. Albright, and K. J. Bowers, in *Modern Challenges in Nonlinear Plasma Physics: A Festschrift Honoring the Career of Dennis Papadopoulos*, AIP Conference Proceedings, Vol. 1320, edited by D. Vassiliadis, S. F. Fung, X. Shao, I. A. Daglis, and J. D. Huba (2010) pp. 144–159.
- [35] W. Daughton, V. Roytershteyn, H. Karimabadi, L. Yin, B. J. Albright, B. Bergen, and K. J. Bower, *Nature Physics* **7**, 539 (2011).
- [36] R. L. Fermo, J. F. Drake, and M. Swisdak, *Phys. Rev. Lett.* **108**, 255005 (2012).
- [37] H. P. Furth, P. H. Rutherford, and H. Selberg, *Phys. Fluids* **16**, 1054 (1973).

- [38] P. K. Kaw, E. J. Valeo, and P. H. Rutherford, *Phys. Rev. Lett.* **43**, 1398 (1979).
- [39] A. Bhattacharjee and E. Hameiri, *Phys. Rev. Lett.* **57**, 206 (1986).
- [40] H. R. Strauss, *Phys. Fluids* **29**, 3668 (1988).
- [41] A. Bhattacharjee and Y. Yuan, *Astrophys. J. Lett.* **449**, 739 (1995).
- [42] H. Che, J. F. Drake, and M. Swisdak, *Nature* **474**, 184 (2011).
- [43] D. Biskamp, *Nonlinear Magnetohydrodynamics* (Cambridge University Press, 1993).
- [44] B. Coppi, E. Galvao, R. Pellat, M. N. Rosenbluth, and P. H. Rutherford, *Sov. J. Plasma Phys.* **2**, 533 (1976).
- [45] Y.-M. Huang and A. Bhattacharjee, *Phys. Plasmas* **20**, 055702 (2013).
- [46] A. Y. Aydemir, *Phys. Fluids B* **2**, 2135 (1990).
- [47] B. B. Kadomtsev and O. P. Pogutse, *Sov. Phys. JETP* **38**, 283 (1974).
- [48] H. R. Strauss, *Phys. Fluids* **19**, 134 (1976).
- [49] H. P. Furth, J. Killeen, and M. N. Rosenbluth, *Phys. Fluids* **6**, 459 (1963).
- [50] P. A. Cassak, M. A. Shay, and J. F. Drake, *Phys. Plasmas* **16**, 120702 (2009).
- [51] R. L. Fermo, J. F. Drake, and M. Swisdak, *Phys. Plasmas* **17**, 010702 (2010).
- [52] R. L. Fermo, J. F. Drake, M. Swisdak, and K.-J. Hwang, *J. Geophys. Res.* **116**, A09226 (2011).
- [53] Y.-M. Huang and A. Bhattacharjee, *Phys. Rev. Lett.* **109**, 265002 (2012), arXiv:1211.6708.
- [54] J. F. Drake, M. Swisdak, H. Che, and M. A. Shay, *Nature* **443**, 553 (2006).
- [55] L.-J. Chen, A. Bhattacharjee, P. A. Puhl-Quinn, H. Yang, N. Bessho, S. Imada, S. Muehlbacher, P. W. Daly, B. Lefebvre, Y. Khotyaintsev, A. Vaivads, A. Fazakerley, and E. Georgescu, *Nature Physics* **4**, 19 (2008).
- [56] J. F. Drake, M. Swisdak, and R. Fermo, *Astrophys. J. Lett.* **763**, L5 (2013).
- [57] A. A. van Ballegoijen and S. R. Cranmer, *Astrophys. J.* **682**, 644 (2008).
- [58] A. Ciaravella and J. C. Raymond, *Astrophys. J.* **686**, 1372 (2008).
- [59] J. Lin, J. Li, Y.-K. Ko, and J. C. Raymond, *Astrophys. J.* **693**, 1666 (2009).
- [60] L.-J. Guo, A. Bhattacharjee, and Y.-M. Huang, *Astrophys. J. Lett.* **771**, L14 (2013).